Feature Article

Stark Realities

Steven G. Boxer

J. Phys. Chem. B, **2009**, 113 (10), 2972-2983• DOI: 10.1021/jp8067393 • Publication Date (Web): 16 January 2009

CENTENNIAL FEATURE ARTICLE

Stark Realities†

Steven G. Boxer*

Department of Chemistry, Stanford University, Stanford, California 94305-5080

Received: July 29, 2008; Revised Manuscript Received: October 20, 2008

Electric fields affect any process or transition that involves the movement of charge. Stark spectroscopy is a general term describing the study of spectral changes in the presence of electric fields, and it has proven to be a broadly useful approach for characterizing the change in dipole moment and polarizability for electronic and vibrational transitions. This article focuses primarily on the evolution of the approach and interconnected applications in diverse fields from our laboratory and prospects for the future. Our work began with studies of chromophores in photosynthetic reaction centers whose function is light-driven charge separation, so perturbations by an electric field were a natural approach. The same methods have been applied to many other biological and nonbiological chromophores. A common theme has been understanding the mechanism(s) of symmetry breaking in molecules or organized assemblies of high symmetry. Spectral shifts in organized systems due to mutations, conformational changes, and ligand binding can, in some cases, be interpreted as Stark shifts. In this case, Stark spectroscopy in a well-defined electric field provides a calibration of the probe transition's sensitivity to an electric field, and the Stark shifts of suitable probes can be used to measure the magnitude and direction of electric fields in proteins, nucleic acids, and membranes. Electric fields can also perturb the populations or reaction dynamics of processes where charge separation occurs. When detected by spectroscopic methods, we call these nonclassical Stark effects. Nonclassical Stark effects arise in the spectroscopy of intervalence charge transfer transitions and both ground- and excited-state electron transfer reactions. Because the movement of charge is ubiquitous in chemistry, biology, and materials science and because electric fields directly affect the energetics of charge-separated species, many phenomena can be viewed as generalizations of the Stark effect.

1. Introduction

Johannes Stark observed splittings of the hydrogen atom Balmer series induced by an electric field nearly 100 years ago,[1] and his name has been associated with this class of effects ever since (despite parallel observations at the same time by Antonino Lo Surdo[2,3]). Measurements of Stark splittings of spectral lines in the gas phase continue to this day, both to obtain fundamental properties of states and transitions and as a diagnostic tool in complex systems such as plasmas. Stark spectroscopy is less widely applied in condensed phases, as large electric fields are needed to detect the effect for inhomogeneously broadened lines. Large fields cause molecular reorientation and dielectric breakdown, and much of the technical development in our laboratory has been to evolve approaches to circumvent these limitations.

In this retrospective article, I consider three aspects of the Stark effect: (i) applications in spectroscopy to experimentally determine the change in dipole moment, $\Delta\vec{\mu}$, and polarizability, $\underline{\Delta\alpha}$, for a transition (classical Stark effects); (ii) the application of classical Stark spectroscopy to calibrate probes, in particular vibrational probes, to investigate electrostatic interactions in organized systems such as proteins; and (iii) the effects of electric fields on the dynamics or populations of species undergoing a chemical reaction, typically detected by spectroscopy (nonclassical Stark effects). Examples of classical Stark effects include both electronic and vibrational Stark effects; nonclassical Stark effects arise naturally in reacting systems where charges are displaced over a considerable distance, such as electron and proton transfer reactions, and where this is detected spectroscopically. Much of our recent work has been concerned with reversing the concept and interpreting observed spectral shifts due to changes in materials (e.g., mutations to amino acids in proteins) as internal Stark shifts. From the analysis of these shifts, we obtain quantitative information on the magnitude and direction of electric fields in organized systems such as proteins or biological membranes that can be compared with simulations. If we broaden the scope to situations where electric fields perturb the properties of a system, then there are a few areas of science where this is not important: field-effect transistors, transmembrane potentials affecting voltage-gated ion channels or driving ATP synthesis, liquid crystal displays, and electrochemistry, to name just a few. With this broader view, it is evident that many of the unique properties of organized materials, whether by human design or natural selection, emerge from the organization and manipulation of electric fields.

Our work grew out of a long-standing interest in the spectroscopy and dynamics of photosynthetic systems. The elementary processes in photosynthesis are photoexcitation, excitation energy transfer, electron transfer, and proton transfer; the latter two are expected to depend strongly on electric fields.

† 2008 marked the Centennial of the American Chemical Society's Division of Physical Chemistry. To celebrate and to highlight the field of physical chemistry from both historical and future perspectives, *The Journal of Physical Chemistry* is publishing a special series of Centennial Feature Articles. These articles are invited contributions from current and former officers and members of the Physical Chemistry Division Executive Committee and from *J. Phys. Chem.* Senior Editors.

* Contact information. E-mail: sboxer@stanford.edu. Phone: 650-723-4482. Fax: 650-723-4817.

10.1021/jp8067393 CCC: $40.75
Published on Web 01/16/2009

Steven G. Boxer received degrees in Chemistry from Tufts University and from the University of Chicago (Ph.D. advisor Gerhard Closs). He has been on the faculty in the Chemistry Department at Stanford University since 1977, where he is currently the Camille and Henry Dreyfus Professor of Chemistry. He is the recipient of the ACS Cope Scholar Award and APS Earle K. Plyler Prize for Molecular Spectroscopy. He is an elected fellow of the American Academy of Arts and Sciences, the Biophysical Society, and the National Academy of Sciences.

We were initially inspired by an abstract from George Feher's group that described an anomalously large effect of an applied electric field on the absorption of the special pair primary electron donor in bacterial photosynthetic reaction centers, although no quantitative analysis was presented.[4] Work from other groups, in particular Richard Mathies in his Ph.D. work with Andreas Albrecht[5] and postdoc with Lubert Stryer[6] building upon earlier work by Liptay,[7] Labhart,[8] and Czekalla,[9] developed methods for quantitative analysis and for enhancing the measurement by linear dichroism to obtain information on both the magnitude and direction of charge transfer associated with a spectroscopic transition. Using this approach with reaction centers in polymer films, we showed that excitation of the special pair breaks the local axis of symmetry observed in the X-ray structure of the reaction center;[10] this example will be discussed in greater depth in section 3.

In an ideal experiment, the molecule or assembly of interest would be oriented relative to the direction of the electric field, for example, in a single crystal, so that both the linear and quadratic Stark effect due to $\Delta\vec{\mu}$ and $\underline{\Delta\alpha}$, respectively, could be directly measured. Robin Hochstrasser[11] and others used measurements of Stark effects in single crystals to provide tests of quantum chemical calculations. However, it is often difficult to obtain a uniaxially oriented sample, especially for a complex biological molecule or assembly. Even in single crystals, it is rare to find just one molecule in the unit cell. Because the Stark splittings or shifts are typically smaller than the inhomogeneous broadening and due to the complication of having several molecules per unit cell, it is difficult to obtain the type of oriented information from well-ordered samples that is familiar to magnetic resonance spectroscopists.

Liptay,[7] Labhart,[8] and Czekalla[9] primarily described the effects of electric fields on electronic transitions for molecules in *fluid* solution. Because most molecules have ground-state dipole moments, application of the field reorients the molecules to some extent. While information can, in principle, be obtained on both the ground and excited dipole moments, only relatively small electric fields can be applied to liquid samples due to dielectric breakdown, so the signal-to-noise is limited and many parameters are convolved in the output of the analysis. Liptay developed the most detailed description; his general equations describing the electronic Stark effect for molecules in fluid solution, while complete, are a bit off-putting with many parameters and many terms.[7] The problem can be tremendously simplified by immobilizing the molecules of interest either in a polymer film or in a frozen glass, though the information extracted is then limited to differences in electro-optic parameters for the states probed by the transition. Frozen glasses include aqueous glasses, typically containing glycerol, so biological samples can be studied under conditions that are not very different from those for X-ray structure analysis. Very large electric fields, on the order of 1 MV/cm, can be applied if the sample is thin enough (typically tens of microns) and free of defects such as bubbles.[12]

I note in passing that "electroabsorption" and "electroemission" are often used interchangeably with the Stark effect, and many papers use these descriptors in their title, especially with electronic and polymeric materials and nanoparticles.

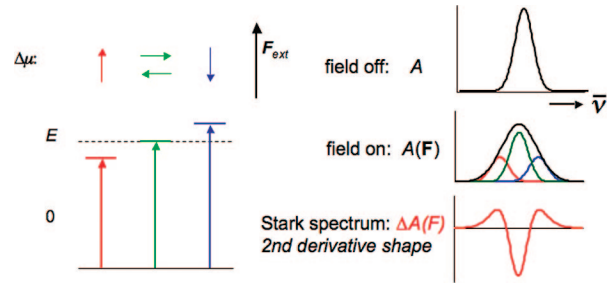

Figure 1. Schematic illustration of the origin of the second derivative line shape for a Stark spectrum of an isotropic, immobilized sample when $\Delta\vec{\mu}$ dominates (eq 7). Vectors corresponding to $\Delta\vec{\mu}$ parallel, antiparallel, and perpendicular to the applied field F_{ext} are shown in red, blue, and green, respectively. The energy in the absence of the field, E, is shifted by $\Delta E = -\Delta\vec{\mu}\cdot\vec{F}_{ext}$ as shown, and the consequence for the spectrum is shown on the right: some orientational subpopulations are shifted to lower energy, some to higher energy, and some remain about the same. The result is a broadened band, and the Stark spectrum is the field-on minus field-off difference spectrum which has the second derivative line shape as shown. In this picture, the spectral shifts are assumed to be much smaller than the inhomogeneous line width; this is nearly always the case for values of $\Delta\vec{\mu}$ found in nature and even for the highest values of the applied field.

2. Classical Stark Effects

In the following, some of the essential relationships used to extract information from Stark spectra for molecules immobilized in a matrix are outlined; much greater detail can be found in the original papers.

For many transitions involving only two electronic or vibrational states, Stark effects are expected to cause a small peak shift in the absorption (or emission) spectrum but no change in line shape; that is, the applied field, $\vec{F}$, perturbs an absorber's transition dipole, $\vec{m}$, and peak position, $\bar{\nu}_{max}$, but neither its population nor its line shape; this is the definition of a *classical* Stark effect. An absorption Stark spectrum, ΔA, is the change in an absorption spectrum under the influence of an applied electric field:

$$\Delta A = A(F\neq 0) - A(F=0) \tag{1}$$

Each absorber's transition polarizability, $\underline{A}$, transition hyperpolarizability, $\underline{B}$, difference dipole moment, $\Delta\vec{\mu}$, and difference polarizability, $\underline{\Delta\alpha}$, are defined by power series expansions truncated at second order in F:

$$\vec{m}(\vec{F}) = \vec{m} + \underline{A}\cdot\vec{F} + \vec{F}\cdot\underline{B}\cdot\vec{F} \tag{2}$$

$$\bar{\nu}_{max}(\vec{F}) = \bar{\nu}_{max} - \Delta\vec{\mu}\cdot\vec{F} - \frac{1}{2}\vec{F}\cdot\underline{\Delta\alpha}\cdot\vec{F} \tag{3}$$

When the ensemble of absorbers is isotropic and the molecules are immobilized, so they do not rotate in the field, and the field perturbations to the individual transitions are small compared to their line widths and intensities, ΔA can be expressed as a sum of the zeroth, first, and second $\bar{\nu}$-weighted derivatives of the absorption spectrum:

$$\Delta A(F,\chi) = f^2F^2\left\{A_\chi \cdot A(\bar{\nu}) + \frac{B_\chi}{15hc}\bar{\nu}\frac{\partial}{\partial\bar{\nu}}\left(\frac{A(\bar{\nu})}{\bar{\nu}}\right) + \frac{C_\chi}{30h^2c^2}\bar{\nu}\frac{\partial^2}{\partial\bar{\nu}^2}\left(\frac{A(\bar{\nu})}{\bar{\nu}}\right)\right\} \quad (4)$$

where the coefficients of zeroth, first, and second derivatives are, respectively,

$$A_\chi = \frac{1}{30m^2}\sum_{ij}[10A_{ij}{}^2 + (3\cos^2\chi - 1)(3A_{ii}A_{jj} + A_{ij}{}^2)] + \frac{1}{15m^2}\sum_{ij}[10m_iB_{ijj} + (3\cos^2\chi - 1)(4m_iB_{ijj})] \quad (5)$$

$$B_\chi = \frac{5}{2}\mathrm{Tr}(\underline{\Delta\alpha}) + (3\cos^2\chi - 1)\left(\frac{3}{2}\underline{\Delta\alpha}_m - \frac{1}{2}\mathrm{Tr}(\underline{\Delta\alpha})\right) + \frac{1}{m^2}\sum_{ij}[10m_iA_{ij}\Delta\mu_j + (3\cos^2\chi - 1)(3m_iA_{jj}\Delta\mu_i + m_iA_{ij}\Delta\mu_j)] \quad (6)$$

$$C_\chi = |\Delta\vec{\mu}|^2\cdot[5 + (3\cos^2\chi - 1)(3\cos^2\zeta - 1)] \quad (7)$$

In these equations, h is Planck's constant and c is the speed of light; $\underline{\Delta\alpha}_m = (\vec{m}\cdot\underline{\Delta\alpha}\cdot\vec{m})/|\vec{m}|^2$; χ is the experimental angle between $\vec{F}$ and the polarization of the probing light field; ζ is the molecule-fixed angle between $\Delta\vec{\mu}$ and $\vec{m}$; and f is a scalar approximation to a tensor called the local field correction (see below). Stark spectra are typically recorded at two or more values of χ and are then fit to a sum of the $\bar{\nu}$-weighted derivatives of the absorption spectrum (eq 4). This procedure essentially redefines A_χ, B_χ, and $\Delta\vec{\mu}$ as fit parameters derived from the coefficients of the zeroth, first, and second derivative components, respectively, of a fit to the Stark spectrum; for example, the fit values of the second derivative contribution as a function of χ are used to determine the magnitudes of $\Delta\vec{\mu}$ and ζ. Note that the same equations apply to emission spectra except that the $\bar{\nu}$-weighting is replaced by $\bar{\nu}^3$-weighting.

Often $\Delta\vec{\mu}$ is the dominant contributor to the Stark effect, and the simple form of the second derivative contribution (eq 7) leads to a simple interpretation of the data. An intuitive view of the origin of the second derivative Stark line shape can be seen by reference to Figure 1. Molecules whose $\Delta\vec{\mu}$ is oriented parallel or antiparallel to the electric field will have their transition energy most shifted to lower or higher energy, respectively; however, most molecules lie at or near the equator so their transition energies are shifted less or not at all. The result is a net broadening of the absorption, and the field-on minus field-off (broadened-minus-not-broadened) line shape has a second derivative shape. This is illustrated in Figure 1 for a symmetric Gaussian band where the symmetric second derivative shape is clear. Most absorption lines are not so symmetric, and this places a premium on high quality absorption spectra, since a rigorous comparison of the line shape of the second derivative of the absorption to the Stark data is needed. To the extent that the transition is polarizable, the applied field induces a dipole and typically this is primarily in the direction of the applied field. Hence, this induced difference dipole mimics a difference dipole in an oriented sample, and the observed effect is a band shift or first derivative line shape (whose sign depends on the sign of the change in polarizability, which is often, but not always, greater in the excited state than the ground state). As seen from eq 6, the first derivative contribution has a complex dependence on several factors, but often the polarizability difference dominates. Note that, for an isotropic sample, all effects scale quadratically with the field due to the orientation averaging (eq 4); hence, the dependence on the field strength, though a useful test that the model is appropriate and the sample is isotropic, is not otherwise useful (it does put a premium on obtaining the highest possible field strength). For ease of comparison, we typically present Stark spectra scaled to a standard value of the external field, typically 1 MV/cm, which is close to the value actually used to obtain the data. Steven Andrews has published an intuitive approach to orientation averaging that the reader may find useful.[13]

It is important to mention several serious limitations that arise in the analysis of Stark effect spectra in condensed phase systems using this approach. First, it is often the case that the signal-to-noise of the absorption spectrum leads to relatively poor signal-to-noise in the derivatives, and since the derivatives of the absorption are used to fit the data, this can be a serious limitation. We introduced a technique called higher-order Stark spectroscopy, discussed briefly in section 3,[14] that can be used to deal with this problem in some cases. Second, typical electronic absorption bands have vibronic structure and the bands are inhomogeneously broadened, and it is not necessarily the case that the same electro-optic parameters apply over the entire band. Stark spectroscopy can be combined with hole-burning to investigate this further, as developed extensively by Wild's laboratory.[119] Third, since ΔA is both positive and negative, the Stark spectra of molecules with overlapping electronic or vibrational transitions with different electro-optic parameters can be quite misleading unless there is a clear model for deconvolving the bands. In some cases, this can be turned into an advantage, for example, in the Stark spectrum of the chromophore that gives green fluorescent protein (GFP) its green color (Figure 2). GFP absorption has two bands, a protonated (A) and deprotonated (B) form of the chromophore,[15] but the Stark spectrum is completely dominated by the relatively narrow and structured absorption of the lower energy deprotonated form. As a result, the spectrum can be deconvoluted to recover the individual contributions of the A and B forms. This is a particularly clear example of a Stark effect that, for the deprotonated B form, is dominated by $\Delta\vec{\mu}$: the Stark spectrum is the second derivative of the absorption, and the much broader A state is absent in the Stark spectrum so we can only place an upper limit on the magnitude of $|\Delta\vec{\mu}|$.[15,16] Note the very close agreement between the Stark spectrum and the second derivative of the absorption for the entire vibronic progression, which demonstrates that the same value of $\Delta\vec{\mu}$ is obtained for the entire band of the B state.

A fourth limitation is the local field correction, a vexing issue in many areas of spectroscopy. The field experienced at any point in space can be approximated as the sum of the matrix field and a term which is proportional to the external field:

$$F_{\mathrm{int}} = F_{\mathrm{matrix}} + f\cdot F_{\mathrm{ext}} \quad (8)$$

The matrix field, F_{matrix}, is the local field in the absence of an applied field; it accounts for the solvent reaction field[17] and for the field due to other organized local structure, such as nearby protein residues. F_{ext} is the average field external to the sample molecule in the nearby solvent (and was simply denoted F in eqs 1−4). The external field is equal to the applied field, which is the applied voltage (known accurately) divided by the electrode spacing (known with moderate precision, typically

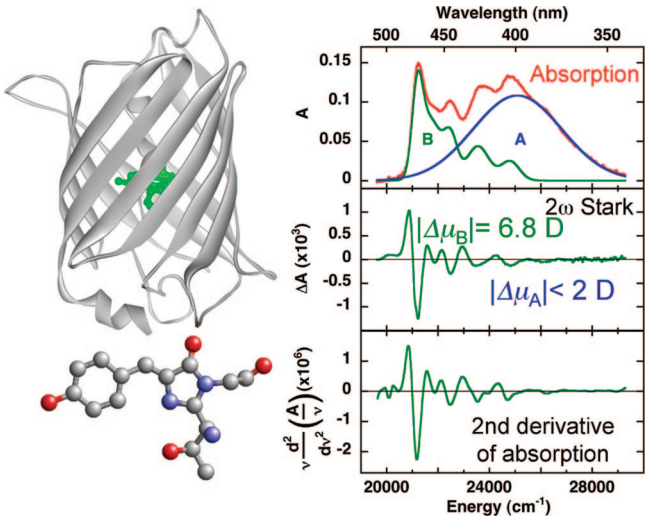

Figure 2. (left) A ribbon diagram of green fluorescent protein (GFP) based on the X-ray structure[117] and the structure of the chromophore that is formed by the spontaneous cyclization and oxidation of three amino acids (Ser65, Tyr66, and Gly67); (right) the absorption (top), 2ω Stark (middle), and second derivative of absorption (bottom) spectra of wild-type GFP[15] (all at 77 K). The lower energy B state (green) is the deprotonated state of the chromophore, and the upper energy A state (blue) is the protonated form.[15] Although these bands overlap, the electronic Stark spectrum is completely dominated by the B state, partly because its features are narrower and partly because $|\Delta\vec{\mu}|$ is considerably greater for the B state than for the A state. This is used to deconvolve the two contributions to the absorption in the top panel, in effect taking the double integral of the Stark spectrum to regenerate the absorption of the B state and then subtracting this from the total absorption to reveal the absorption of the A state.

from interference fringes in the sample). The local field correction factor, f, is a tensor in a general treatment but is typically approximated by a scalar for simplicity. Also, the inhomogeneity of f within the volume of a chromophore and the variability of f between different chromophore molecules are typically ignored (it is also assumed that the external field does not affect F_{matrix}, which is reasonable in a frozen glass sample). It is sometimes expedient to largely side step the local field issue by reporting results in terms of f. For example, linear Stark effects can be given in units of Debye/f and quadratic Stark effects in units of $\text{Å}^3/f^2$. This is useful for a comparison of results between samples dissolved in similar solvents, because f, while unknown, is expected to remain nearly constant. While useful for comparisons among a series of related molecules, comparisons with *ab initio* gas phase calculations are compromised by uncertainties in f. Many models are available for the local field correction, all depending on the dielectric constant of the solvent.[17] While the values of the dielectric constants of liquid solvents have a wide range, those of frozen solvents are not that different (for example, the capacitance of samples with different frozen solvents are comparable and the corresponding dielectric constants are relatively small, on the order of 2−3). Therefore, the variations in f for the frozen solvents used in Stark measurements are not likely to be large, and values of f between 1.1 and 1.3 are calculated irrespective of the model[17] used to estimate f.

3. Examples of Classical Stark Effect Spectra

In this section, I highlight a few examples from our laboratory where classical Stark spectroscopy has been most useful. The setup for measuring Stark spectra is quite simple, though a few tricks are essential to obtain high quality data.[12] The sample is held in a thin (tens of microns) cell using spacers to separate windows made from glass, quartz, sapphire, CaF_2, or ZnSe depending on the region of the spectrum. Electrodes are deposited on the inner surface. A thin (∼40−70 Å) film of Ni has a reasonable transmission over a wide region of the spectrum, or indium-tin-oxide (ITO) can be used. The key is to rapidly freeze the sample without creating bubbles or strain, so a glass-forming solvent is essential. Because there is a small amount of resistive heating in the electrodes, heat dissipation is essential and is best accomplished by direct immersion in liquid nitrogen. A liquid nitrogen immersion cryostat that can be refilled without disrupting the sample has been developed,[18] and this is ideal for all types of Stark measurements.

Since the signals are small, when possible, it is desirable to use lock-in detection by locking onto the harmonics of the field-modulation frequency. The conventional method uses the second harmonic of the field-modulation frequency ω (the "2ω spectrum", where ω is typically a few hundred hertz). This has been extended to the higher even harmonic responses of the absorption to the applied AC field (the odd harmonics should be zero), a technique we called higher-order Stark spectroscopy (HOSS).[14] The field-induced change in absorbance by an externally applied sinusoidal electric field, $F(\omega) = F_0 \sin(\omega t)$, is given by

$$\Delta A(\nu, F) = \Delta A(\nu, F^2, 2\omega) + \Delta A(\nu, F^4, 4\omega) + \Delta A(\nu, F^6, 6\omega) + \ldots \quad (9)$$

The individual terms of this series can be recorded using lock-in detection at the second, fourth, sixth, etc., harmonic of the field-modulation frequency ω, with the nth-order spectrum depending on the nth power of the applied field F^n. An expression can be obtained for each nth-order spectrum,[14] with the ΔA signal equivalent to a sum of zeroth through nth derivative terms. If $\Delta\vec{\mu}$ dominates the Stark spectrum, the $(n+2)$th-order Stark spectrum is proportional to the second derivative of the nth-order spectrum. This diagnostic is useful because Stark spectra (and thus their derivatives) can often be obtained with better signal-to-noise than the derivatives of the absorption spectrum. An example for the case of bacteriochlorophyll *a* is shown in Figure 3,[14] where the 2ω and 4ω spectra are compared with the second derivative of the absorption and the second derivative of the 2ω spectrum, respectively. In the bacteriochlorophyll *a* case, $\Delta\vec{\mu}$ dominates the Stark effect, and the second derivative line shape for the 2ω spectrum is evident, as is the fourth derivative shape of the 4ω spectrum. Furthermore, because a numerical multiplier relates the amplitude of the 2ω and 4ω spectra when $\Delta\vec{\mu}$ dominates, the ratio of the intensities of the higher-order Stark spectra provides both an independent check on the value of $\Delta\vec{\mu}$ and a diagnostic that $\Delta\vec{\mu}$ dominates.

The case of bacteriochlorophyll *a* is important since much of our work has involved photosynthetic reaction centers (RCs) whose absorbing and reacting pigments are bacteriochlorophylls, as shown on the left side of Figure 4. The elucidation of the three-dimensional structure of the bacterial RC was a landmark in structural biology and completely transformed research in this area.[19,20] The most striking finding, seen clearly in the schematic derived from the structure in Figure 4, is a high level of symmetry: rotation about a vertical axis by 180° generates a chromophore arrangement that is nearly indistinguishable, yet this local C_2 symmetry is broken at the level of function: following excitation of the special pair, P, a dimer of two strongly interacting bacteriochlorophylls, electron transfer occurs only along the "L-branch" of chromophores, $^1P \rightarrow P^+B_L^- \rightarrow$

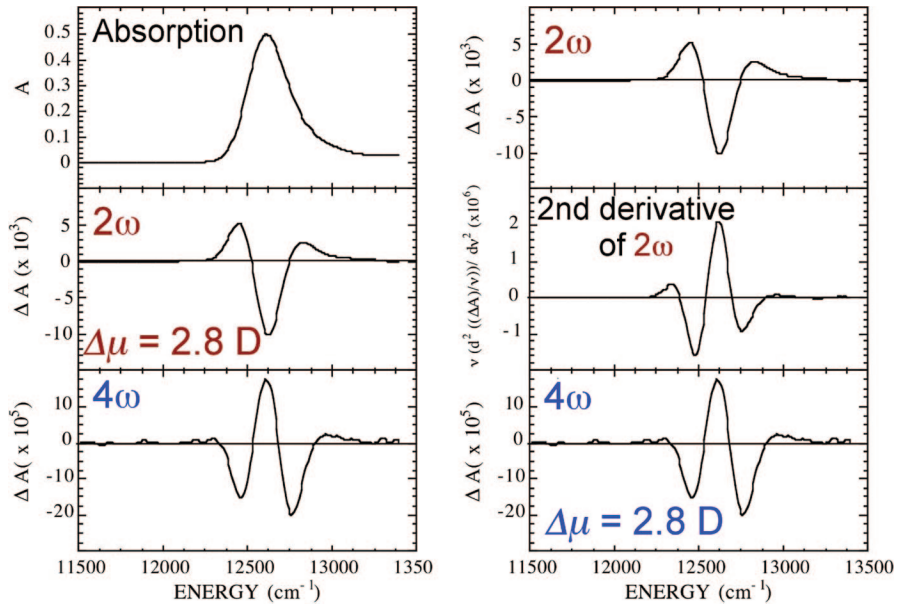

Figure 3. (left) Absorption (top), 2ω (middle), and 4ω (bottom) electronic Stark spectra of bacteriochlorophyll *a* in 2-MeTHF at 77 K; (right) the second derivative (middle) of the 2ω Stark spectrum (top) is compared with the 4ω Stark spectrum (bottom). The line shape of the second derivative of the 2ω spectrum is similar to the 4ω spectrum; the ratio of the 2ω and 4ω spectra can be used to extract $|\Delta\vec{\mu}|$, and this is compared with the value from a conventional analysis of the 2ω Stark spectrum based on the second derivative of the absorption spectrum.

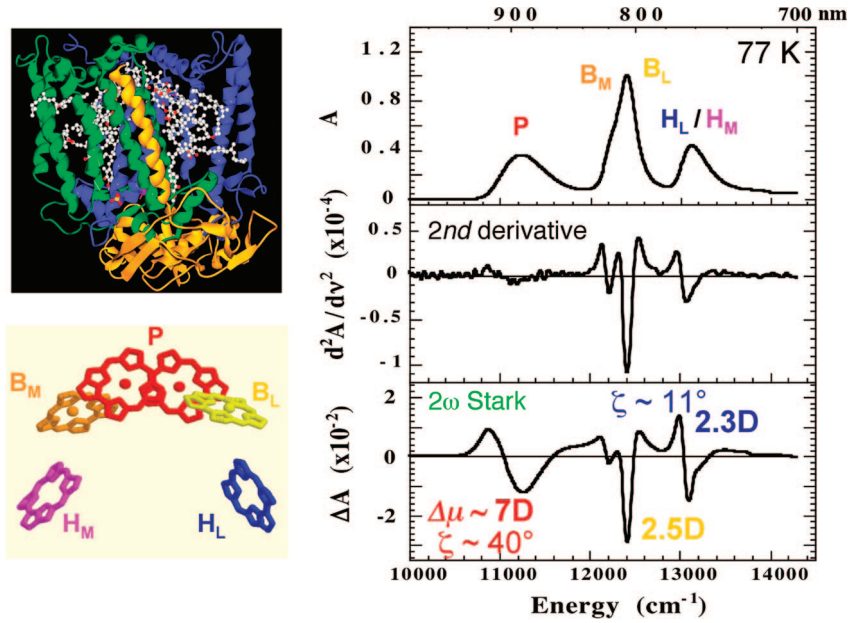

Figure 4. (left) Three-dimensional structure of the bacterial reaction center from *Rb. sphaeroides* (top) and the reactive chromophores (bottom).[20] (right) The absorption (top), second derivative of absorption (middle), and electronic Stark spectrum (bottom) at 77 K (the bands are assigned and color coded according to the diagram on the lower left).[10,22] The second derivative of the broad absorption of the special pair primary donor (P) is hardly seen because the band is broad; nonetheless, a strong electronic Stark effect is seen, so $|\Delta\vec{\mu}|$ for P must be large; by contrast, $|\Delta\vec{\mu}|$ for the monomeric bacteriochlorophylls (labeled B) and bacteriopheophytins (labeled H) are similar to their value in an organic glass (c.f. Figure 3 for bacteriochlorophyll *a*).

$P^+H_L^-$, with no evidence for electron transfer along the M-branch of chromophores.[21] The absorption spectrum of the lowest energy electronic transitions for these six chromophores is shown on the right (upper panel) with their simplest assignment. The comparison of the Stark spectrum in the lower panel with the second derivative of the absorption in the middle panel is striking: the Stark effect for the P band is much larger than for the monomeric chromophores[4,10,22] even though the P band is broader than the other bands and so its second derivative is much smaller (this is an excellent example of the difficulty of analyzing Stark data by taking derivatives of the absorption for which HOSS is very useful[14]). Quantitative analysis shows that the magnitude of $\Delta\vec{\mu}$ is substantially larger for dimeric P than for the monomeric chromophores from which it is formed, whose values are comparable to those of the pure chromophores isolated in an organic glass (c.f. Figure 3; further analysis shows that the situation is considerably more complicated, as the polarizability change is also much larger for P than for its constituent monomers[23]). Furthermore, the measured angle ζ between $\Delta\vec{\mu}$ and the transition moment is substantially larger for P than for the monomeric chromophores, whose value again is very similar to that found for the pure chromophores isolated in an organic glass.[10,14,22] The simplest interpretation of these results is that the lowest excited state of the special pair P has

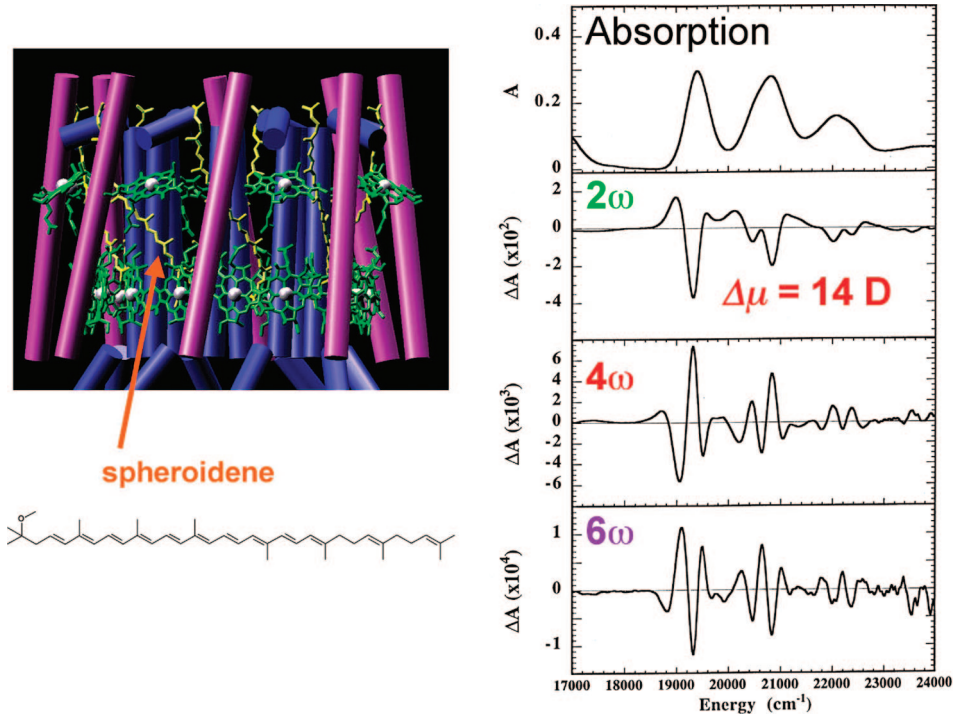

Figure 5. (left) Model derived from the X-ray structure of the LH2 (light-harvesting 2) antenna complex[25] adapted from ref 113. The red and blue cylinders represent transmembrane alpha helices that hold the bacteriochlorophylls (green) and the carotenoid spheroidene (yellow, structure shown) rigidly in place. Rings of LH2 antenna complexes funnel energy to the reaction center via another antenna that surrounds the reaction center. (right) Absorption (top panel), 2ω, 4ω, and 6ω electronic Stark spectra of the vibronic bands associated with spheroidene in the LH2 complex.[14] The 2ω spectrum closely matches the second derivative of the absorption, and the higher-order Stark spectra are each second derivatives of the $(n-2)$th-order Stark spectra. The extracted value of $|\Delta\vec{\mu}|$ is 14 D, much larger than expected for a nearly inversion symmetric chromophore (see text).

a much greater degree of charge transfer character than its constituent monomers, and that this charge transfer breaks the symmetry of the reaction center.[10,24]

Another interesting example comes from a second important chromophore-containing protein complex in the photosynthetic membrane, the antenna complex. Most of the chlorophyll in photosynthetic membranes is associated with antenna complexes. The antenna complexes consist of organized assemblies of chromophores held in place by the antenna proteins and function to greatly enhance the absorption cross section for solar irradiation and to efficiently funnel excitation energy to the RC where charge separation occurs. The structures of many of these antenna complexes have now been obtained. The so-called LH2 complex from photosynthetic bacteria[25] is illustrated on the left in Figure 5. LH2 and other antenna complexes in certain bacterial species occur as rings containing repeating subunits of simple transmembrane alpha helices (shown as purple and blue cylinders) decorated with bacteriochlorophylls (shown in green). While the Stark spectra of the chlorophylls have been studied in several antenna complexes,[26−28] the most striking result is the Stark spectrum of a bound carotenoid, spheroidene (yellow in the diagram).[29,30] As seen in the structure of spheroidene, the conjugated system nearly has inversion symmetry; thus, a small value of $|\Delta\vec{\mu}|$ is expected. Polyenes have highly polarizable excited states; thus, a substantial value of $\underline{\Delta\alpha}$ is expected; consistent with this, the Stark spectrum of isolated spheroidene in an organic glass is dominated by a first derivative line shape.[29,30] What is striking, then, is the complete dominance of a second derivative line shape for spheroidene *in the antenna complex* (note this extends over the well-resolved vibronic structure, Figure 5, right). Furthermore, the 4ω spectrum is almost exactly the second derivative of the 2ω spectrum, the 6ω spectrum the second derivative of the 4ω spectrum (and the fourth derivative of the 2ω spectrum), and so on (we have measured this up to the 12ω spectrum), and the magnitude of $|\Delta\vec{\mu}|$ is 14 D!

How can a molecule which should have only a small value of $|\Delta\vec{\mu}|$ by symmetry exhibit such a large value of $|\Delta\vec{\mu}|$? Our interpretation is that the electric field created by the organized environment in the antenna protein around the carotenoid induces a substantial $\Delta\vec{\mu}$ in the highly polarizable polyene. As seen in the three-dimensional structure,[25] the spheroidene molecules have a very regular arrangement in the LH2 complex, and the sharp vibronic structure is consistent with this. Thus, each spheroidene could experience a similar field, since each is in a similar environment, but of course, you cannot "see" the field in the structure; rather, the molecule senses the field.

This example is instructive for several reasons. First, it led us to use Stark spectroscopy to investigate electronic consequences of the internal fields created by groups covalently attached on the ends of polyenes. Many "push−pull" polyenes with electron donors and acceptors at opposite ends have been created because of their unusual nonlinear optical properties. Working with Seth Marder, we systematically investigated the Stark spectra of a range of examples from this class of compounds and could make connections with other spectroscopic methods, the results of electronic structure calculations, and models for nonlinear optical properties that depend upon $\Delta\vec{\mu}$;[31−33] related work has been reported by other groups.[34,35]

Second, the specific case of spheroidene in LH2 helps to settle a long-standing ambiguity in the literature on transmembrane potentials. Biological membranes are roughly 5 nm thick and very good insulators. Transmembrane potentials can be created by transporting cations or anions across the membrane (pho-

tosynthetic electron transfer drives proton transport across the membrane through a series of membrane-bound enzymes), and these potentials are used to drive important biological reactions such as the synthesis of ATP.[36] The magnitude of the transmembrane potential is therefore of great importance. Early observations in photosynthetic membranes showed an "electrochromic band shift" of carotenoid molecules in antenna complexes (similar to spheroidene in LH2) when the transmembrane potential was changed by illumination. As the apparent potential was increased by more intense illumination, the band shift increased linearly with intensity.[37] This was a puzzle because it was well-known at the time that polyenes are highly polarizable, but since it was presumed that the carotenoid has a fixed and uniaxial relationship with the transmembrane potential, a quadratic Stark shift (eq 3) was expected as the transmembrane potential increases, contrary to observation. Various attempts to interpret a parabola as a line ensued (!), but it is clear from the data in Figure 5 that spheroidene in the antenna complex does indeed have a very large $|\Delta\vec{\mu}|$. This induced $\Delta\vec{\mu}$ is uniaxially oriented relative to the electric field from the transmembrane potential because the antenna complex itself is well oriented in the membrane, and thus, the absorption of the bound polyene should exhibit a *linear* shift with increasing transmembrane potential. This example shows that the measurement of the Stark effect spectrum for an isolated, nonoriented antenna complex in an external field provides a calibration for the sensitivity of this chromophore in this assembly when it is oriented relative to a transmembrane electric field. Note that investigators in bioenergetics and neurobiology apply this concept daily by the use of "voltage sensitive dyes".[120] These dye molecules, which typically have a substantial intrinsic $\Delta\vec{\mu}$, insert into membranes, and their spectra shift to higher or lower energy as the transmembrane potential changes; the underlying mechanism is a Stark effect, and these transmembrane potential changes can be visualized with high temporal and spatial resolution using advanced imaging methods.

Third, the concept of the Stark experiment for spheroidene in LH2 was used in a different way to probe dielectric screening in the bacterial reaction center. Following light excitation, charge is separated over 25 Å in several steps from the excited state of the special pair P to a quinone, Q_A, that is also on the "L-side" of the RC to form $P^+Q_A^-$ which lives for hundreds of milliseconds (Q_A is not shown in Figure 4, it is directly below H_L). The electric field due to this transient light-induced internal charge-separated state is expected to be larger for the L-side monomeric chromophores, B_L and H_L, than for the more distant B_M and H_M; consequently, Stark band shifts due to the $P^+Q_A^-$ field should be larger for B_L and H_L than for B_M and H_M (geometric factors also enter). However, the opposite is observed; hence, the field is screened to a greater extent on the functional L-side than on the nonfunctional M-side, and this may contribute to the functional asymmetry for light-driven electron transfer in the reaction center.[38]

Fourth, this observation stimulated our interest in learning more about the magnitude of the electric fields that are present in organized systems like the LH2 complex. In principle, it should be possible to turn the experiment around and extract information on the protein electric field from the induced dipole that is observed. This is complicated for spheroidene in LH2, since the polarizability tensor of the polyene must be known, and the polyene extends over a large volume of the protein; to date, this calculation has not been attempted. A more specific concept has been used to understand the origin of color tuning of the visual pigments, particularly the early work of Barry Honig, who calculated the effects of charged amino acids on the retinal absorption in rhodopsin[39] (and who correctly anticipated the results for spheroidene[40]). This evolved to Honig's calculations and graphical representations of protein electrostatic potentials that accompany nearly every protein X-ray structure, typically as red, white, and blue electrostatic potential maps.[41] Such pictures guide our intuition about sites on protein surfaces where electrostatic complementarity may play an important role in guiding protein−protein, protein−DNA, protein−ligand, or protein−membrane interactions. A quantitative analysis shows that protein electrostatics may have a profound impact on catalysis in enzymes, a view most strongly articulated by Arieh Warshel.[42] The problem is that binding constants or catalytic rates are a very indirect measure of the electrostatic potential or its gradient, the electric field. Stark shifts should provide a sensitive local and directional probe of these fields, and this led us to the concept that vibrational Stark effects might be more useful than electronic spectral shifts for probing electric fields in proteins.

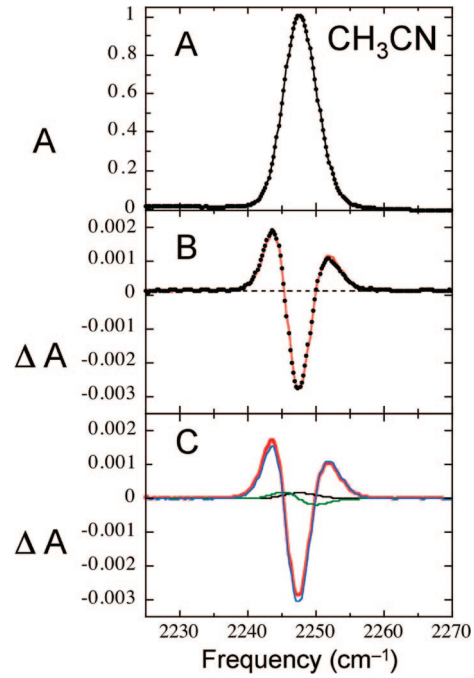

Figure 6. Vibrational Stark spectrum of acetonitrile in 2-MeTHF, at 74 K.[44] (A) Extinction coefficient spectrum of the nitrile stretch mode; (B) vibrational Stark data (dots, scaled to 1 MV/cm applied field) and the best fit to the Stark spectrum, using numerical derivatives of the data in panel A (solid line); and (C) decomposition into sum (red) of derivative components (blue, second derivative; green, first derivative; black, zeroth derivative). The second derivative dominates, and the value of the Stark tuning rate is 0.43 cm^{-1}/(MV/cm).

At the time we began to study vibrational Stark effects, there were only a handful of examples in the literature, nearly all in the gas phase. Vibrational Stark effects are expected to be small: for a harmonic oscillator, the average position of the oscillator is the same for each level so there is no charge displacement upon making a transition. Of course, real bonds are anharmonic, and the field may affect the force constant for the oscillator, so we set out to see whether these effects are measurable. As shown in Figure 6, it is straightforward to measure the vibrational Stark effect even though $|\Delta\vec{\mu}|$ is only a few hundredths of a debye because the inhomogeneous line widths are typically quite small ($\sim$10 cm^{-1}; the relatively narrow line widths are, of course, related in part to the small $|\Delta\vec{\mu}|$).[43−45] Lock-in detection is possible using a dispersive spectrometer[43] or a step-scan system

TABLE 1: Bond Types, Frequencies, Intensities, and Stark Tuning Rates of Relevant Functional Groups[48] [a]

bond type	$\bar{\nu}$ range, cm^{-1}	intensity	Stark tuning rate, $\lvert\Delta\vec{\mu}\rvert$, $cm^{-1}/(MV/cm^{-1})$
−C−H	2850−3100	weak	0.2−0.6
−C−D	2000−2200	weak	0.4−1.5
−C−F	1100−1300	strong	0.4−0.9
carbonyl	1600−1750	strong	0.6−1.8
−C≡N	2050−2270	strong	0.4−2.9
azide	2080−2170	very strong	small
−N=C=O	2250−2300	very strong	small
nitro	1490−1600	strong	∼1.3
−Si−H	2100−2200	medium	∼2.3

[a] On the basis of these results, the −C≡N functionality is most promising. C−F and NO_2 stretches are intense and sensitive to electric fields but fall in a cluttered region of the protein's absorption spectrum. Organic azides are intense but relatively insensitive to electric fields, and their spectra are often complicated. −C−D is in a good spectral region, but the intensity is weak; $-CD_3$, as in CD_3-methione has been used,[65] but this is complicated since multiple projections of the electric field are sampled.

on an FTIR; however, we have found that DC application of the field is superior on the FTIR.[46] A comprehensive analysis of the vibrational Stark effect for nitriles (the C≡N stretch around 2200−2300 cm^{-1}) partitions contributions from bond anharmonicity and electronic perturbations of chemical bonds.[44,45] For a localized oscillator like C≡N, the direction of $\Delta\vec{\mu}$ is expected and found to be parallel to the transition moment direction (i.e., $\zeta \approx 0°$), and since the transition moment is parallel to the C≡N bond axis, both the magnitude and direction of $\Delta\vec{\mu}$ are known (its sign can be inferred from chemical arguments[47]). It is useful to recast values of $|\Delta\vec{\mu}|$ as a Stark tuning rate with units of $cm^{-1}/(MV/cm)$; thus, the Stark tuning rate quantifies or calibrates how much of a shift (in wavenumbers) is expected for a 1 MV/cm projection of the electric field on the bond axis. Table 1 summarizes Stark tuning rates for several classes of vibrations that might be useful probes for biological systems.[48]

These results suggest using vibrational frequency shifts as a probe for electric fields in complex organized systems. If the Stark tuning rate is an intrinsic property of the probe oscillator, then placing the oscillator in different matrix electric fields should shift the observed spectrum according to the projection of the matrix (e.g., protein) field on the bond direction:

$$hc\Delta\bar{\nu}_{obs} = -\Delta\vec{\mu}_{probe}\cdot\Delta\vec{F}_{protein} \quad (10)$$

where $\Delta\bar{\nu}_{obs}$ is the observed frequency shift in wavenumbers, h is Planck's constant, c is the speed of light, and $\Delta\vec{F}_{protein}$ is the change in field at the probe vibration between two states of the protein, for example, two conformational states, protonation states, or two mutants. While it is not possible to apply an external electric field much larger than 1 MV/cm without dielectric breakdown, based on electrostatics calculations, the variations in fields within proteins and nucleic acids can be as large as ±30 MV/cm,[41] so substantial vibrational frequency shifts might be seen given the Stark tuning rates reported in Table 1.

We first introduced the vibrational probe concept for the analysis of shifts observed in mutants and protonation states of carbon monoxide bound to heme iron in myoglobin (Mb).[49] Our laboratory cloned the gene for human Mb[50] with the aim of creating mutants that would produce spectral shifts of bound chromophores such as chlorophylls[51] (inspired by Honig's work on the visual pigments, we thought a similar concept might be important in photosynthetic systems; it probably is not) or heme iron redox potentials.[52,53] Many laboratories created Mb mutants, often in the vicinity of the site near the heme iron where diatomic ligands bind, and for carbon monoxide or nitric oxide, large IR spectral shifts were observed for the bound diatomic in these mutants. The Stark tuning rate for carbon monoxide bound to the heme iron in the protein is unusually large,[49] and the spectral shifts in mutants could be interpreted as having a large contribution from local perturbations to the electrostatic potential.[49,54−56] However, when compared with predictions of spectral shifts from electrostatics calculations, while the trends were correct, the quantitative agreement was rather poor.

Carbon monoxide bound to heme is hardly a general probe for electrostatics in proteins, but referring to the data in Table 1, it is evident that −C≡N, −C−F, or −C−D could be a useful and more general probe (−C−D offers the smallest chemical perturbation but suffers from a low extinction coefficient). Of course, none of these oscillators occur naturally in proteins or nucleic acids, but −C≡N and −C−F moieties are surprisingly common in drugs and inhibitors, so one strategy is to perturb the environment around the site where a ligand displaying a −C≡N or −C−F binds, measure the spectral shift, and compare this result with predictions from electrostatics calculations.[47,57] Nitriles can be introduced site-specifically into proteins by a simple modification of cysteine residues to form thiocyanates, −S−C≡N,[58] and this has been used to probe electrostatics at the active site of the enzyme ketosteroid isomerase.[59] Nitrile-containing nucleic acids are now available and can be site-specifically inserted into DNA sequences.[60,61] More generally, probes such as *p*-cyano-phenylalanine or *p*-fluoro-phenylalanine can be introduced site-specifically into proteins by total synthesis,[62,63] protein semisynthesis,[58] or nonsense suppression.[64,65] None of these methods is simple yet, and these non-natural vibrational probes may have environment-specific interactions that alter $\Delta\vec{\mu}$ (this can be checked by measuring the vibrational Stark effect for the probe in the protein[49,58]) or the probe may impact the electrostatic fields it is meant to test. Each of these approaches has been used to probe electrostatics in several proteins and to compare the observed spectral shifts with those predicted by electrostatics calculations. While detailed examples can be seen in the original papers, we typically find that the magnitudes of the electric fields sensed by the vibrational Stark probes and the calculated values are very different unless high resolution structures are available and extensive molecular dynamics is used to obtain a realistic value of the time-averaged electric field.[57] Developing methods to predict electric fields within proteins is currently an active area of research in our laboratory and others,[65] and it remains to be seen whether the vibrational Stark shifts can impact the parameters used in electrostatics calculations.

4. Nonclassical Stark Effects

Nonclassical Stark effects are distinguished from classical Stark effects by the dependence of some *process* on the applied electric field in addition to the spectral shifts that were described above. Because dynamics are affected, the line shapes that result can be very different from the simple sums of derivatives described for classical Stark spectroscopy. In nearly every case, we stumbled into an example while probing some feature of the photosynthetic reaction center; the detailed results and underlying theories can be found in the original papers; here, I

summarize only the key concepts. The simplest (in concept at least) example is the fluorescence Stark effect for a molecule where some electric-field-dependent nonradiative process competes with fluorescence. For example, consider a fluorescent electron donor D that participates in an excited-state electron transfer reaction with electron acceptor A. In the absence of A, the fluorescence Stark effect from the excited state, ^{1}D, should mirror that of the absorption of D. However, when the acceptor is present, an excited-state electron transfer reaction can occur, $^1DA \rightarrow D^+A^-$, and the rate of this process can be described by Marcus theory or one of its descendants.[66] While excitation of or emission from D in the absence of A may involve a change in dipole moment, $\Delta\vec{\mu}$, giving a classical absorption or fluorescence Stark effect, respectively, the product of electron transfer, D^+A^-, will have a *huge* dipole moment; the difference between this dipole moment and that of ^{1}D is denoted $\Delta\vec{\mu}_{CT}$, where CT denotes charge transfer and typically $\Delta\vec{\mu}_{CT} = \vec{\mu}_{D^+A^-} - \vec{\mu}_{1_D} \approx \vec{\mu}_{D^+A^-}$. For an isotropic sample, all orientations of $\Delta\vec{\mu}_{CT}$ are present: some will be parallel to the applied electric field, and so the energy of the D^+A^- state will be shifted down relative to the value in the absence of the applied electric field; conversely, some will be shifted up and, as in the left side of Figure 1, many will be relatively unaffected. These energy shifts translate into changes in the driving force for the electron transfer reaction, and electron transfer theory predicts a strong nonlinear dependence of the *rate* of electron transfer on driving force. Thus, the rate of the $^1DA \rightarrow D^+A^-$ charge transfer reaction will be different for different orientational subpopulations in the sample; some rates will be faster than at zero applied field, some slower, depending quantitatively on the mapping between driving force and rate. As a result, the quantum yield of fluorescence that competes with this electric-field-dependent process will be affected. These effects are likely to greatly increase or decrease the fluorescence intensity depending on the curvature of the rate vs driving force curve around the zero applied field value, and this can be orders of magnitude larger than the classical Stark effect. The classical fluorescence Stark effect is still present, and the combination produces large changes in intensity and/or line shape for steady-state emission spectra that cannot be analyzed using the classical derivative decomposition.[67−69] These electric field effects can also be observed directly as a change in kinetics by time-resolved absorption[70−74] or fluorescence. Furthermore, because different orientational subpopulations react at different rates, the competing fluorescence from an isotropically excited sample should become polarized, as the greatest contribution to the fluorescence will be from that orientational subpopulation whose electron transfer rate slows the most[75,76] and this can be used to estimate the projection of $\Delta\vec{\mu}_{CT}$ on the fluorescence transition dipole moment of D, a molecule-fixed direction. The example given here is an excited-state electron transfer, but population effects can exist in the ground state as the energies of states shift in an electric field, as illustrated in Figure 7A.[77] Many nonbiological examples of fluorescence electric field effects from distributions of donors and acceptors in films have been published by Ohta's laboratory.[121,122]

A coupled kinetic/spectroscopic effect on excited-state electron transfer is accompanied by a second, subtler, nonclassical Stark effect on the absorption of the donor. In order for electron transfer to occur, there must be mixing between ^{1}D and D^+A^-. Mixing is typically smaller than the inhomogeneous broadening and is not directly observable in the absorption of D. However, the mixing is present, and it too will be affected by the applied electric field, again because the energy of the coupled D^+A^- product state depends strongly on electric field. Thus, the absorption Stark effect of the donor, in addition to the classical contribution described earlier, will experience a nonclassical contribution whose line shape depends upon the same electron transfer parameters described above. We have called these "resonance Stark effects" (Figure 7B), and they have been observed thus far only for a particular reaction in photosynthetic reaction centers.[78−81] The theory describing these effects is complicated,[79,80] but radically different line shapes from the classical derivative line shapes (eqs 1−4) are predicted. These effects are mostly easily observed using the higher-order Stark method, since the classical contribution drops rapidly in higher-order spectra, while the resonance Stark contribution has a weaker decline. Many unusual resonance Stark line shapes have been observed in different reaction center mutants; these can be simulated using the full theoretical treatment to extract information on the driving force, reorganization energy, and electronic coupling. This is a purely spectroscopic approach to these parameters, rather than the usual approach through the interpretation of kinetics. The general utility of resonance Stark spectroscopy as an alternative to kinetic measurements is probably limited because the Stark experiment is performed on frozen glasses, and many light-driven electron transfer reactions in model donor−acceptor systems stop when the solvent is frozen.

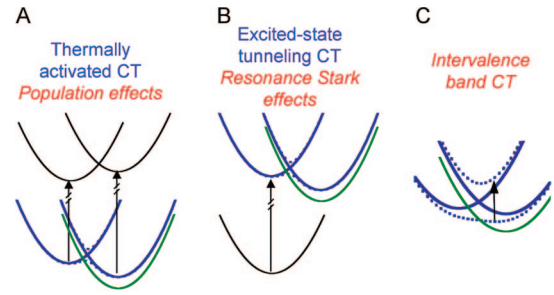

Figure 7. Schematic energy level diagrams illustrating three types of nonclassical Stark effects in which the absorption or emission line shape is affected.[77] In each case, the levels in blue are in the absence of the applied field and a shift in level is given (green) for one orientation of the field. (A) For population effects, application of the field shifts one of the states to lower energy and so the populations are expected to respond as the system returns to equilibrium. (B) A similar effect is expected for excited-state electron transfer. The charge-separated-state energy is shifted by the field changing the rate of electron transfer. The electric field also affects the ground-state absorption due to mixing of the locally excited and charge-separated states leading to "resonance Stark effects". (C) Intervalence charge transfer bands correspond to direct transfer of an electron from one part of a molecule to another. The intensity, position, and line width of these transitions can be described by Hush[82] or PKS[83] theory, and application of a field is expected to shift the relative energy of the states involved in the transition, leading to unusual intervalence band Stark effect line shapes.

A third example of a nonclassical Stark effect is illustrated in Figure 7C for intervalence charge transfer transitions. Mixed-valence systems involve two or more states with different electric dipole moments whose magnitudes depend upon the charge transfer distance and the degree of delocalization; these states can be interconverted by excitation of an intervalence charge transfer transition whose intensity, position, and width depend on the driving force, reorganization energy, and electronic coupling as described by Hush[82] or PKS[83] theory. Since Stark spectroscopy involves the interaction between the change in dipole moment of a transition and an electric field, the Stark spectra of intervalence charge transfer transitions are expected to provide quantitative information on the degree of

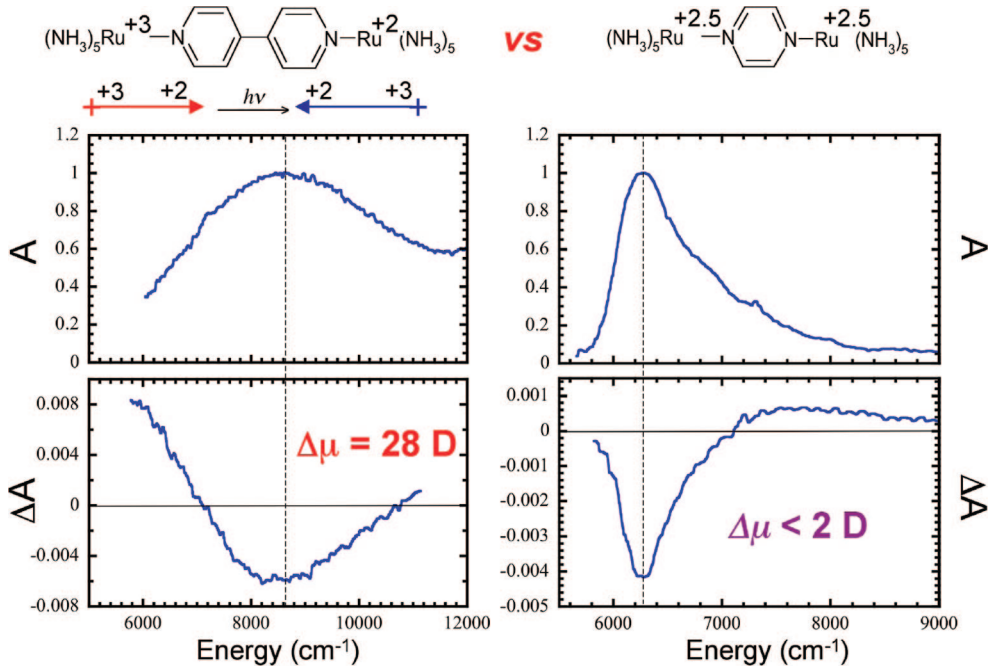

Figure 8. Two mixed-valence complexes based on Ru^{2+}/Ru^{3+} bridged by different ligands, 4,4′-bipyridyl on the left and bipyridyl (the Creutz−Taube ion) on the right.[84,85] For the larger ligand, the valence is expected to be fully trapped (localized). Intervalence charge transfer converts the Ru^{2+}-L-Ru^{3+} ground state into the Ru^{3+}-L-Ru^{2+} excited state whose large dipole points in the opposite direction; thus, $|\Delta\vec{\mu}|$ is expected to be large. For the Creutz−Taube ion, the metal centers are much more strongly coupled because the ligand is smaller, so the intervalence transition is expected to reflect greater delocalization. Accordingly, the ground- to excited-state transition does not exhibit a large $|\Delta\vec{\mu}|$. This simple concept is born out by the Stark spectra analyzed using classical Stark theory. A more sophisticated analysis using a full nonclassical analysis yields similar values for the extreme case of the 4,4′-bipyridyl ligand but a refined view of charge transfer in the Creutz−Taube ion.[93,96]

delocalization that is independent of and complements the analysis of the absorption alone.

Two classic examples of mixed-valence systems based on Ru^{2+}/Ru^{3+} with different bridging ligands are shown in Figure 8. In the case of the bipyridyl ligand on the left, the coupling between the metal centers is attenuated by the length of the ligand. As illustrated, the intervalence charge transfer transition converts a large ground-state dipole moment into a large excited-state dipole pointing in the opposite direction, so $\Delta\vec{\mu}$ (in the sense of classical Stark spectroscopy) is expected to be large and parallel to the direction of charge transfer ($\zeta = 0°$). In the famous Creutz−Taube ion shown on the right, the smaller ligand leads to much stronger coupling between the metal centers and thus the possibility of delocalization where the effective valence on each metal is +2.5. In this case, the mixed-valence system resembles a delocalized aromatic molecule, and so $\Delta\vec{\mu}$ for the intervalence charge transfer band should be small. The experimental results and classical analysis provided a semiquantitative approach for the analysis of the degree of delocalization in these mixed-valence systems which had, especially for the Creutz−Taube ion, been the subject of much controversy.[84−86] Hupp's group has done related work on other mixed-valence systems.[87−92]

In the most interesting intermediate cases between localized and delocalized, the analysis should be much more complex because the field affects not only the band position but also the intrinsic band shape. As with the description of the resonance Stark effect above, the full theory is complex,[93] but the basic concept can be understood by reference to Figure 7C. Because the energy of the difference dipole moment, $\Delta\vec{\mu}_{CT}$, depends on its orientation in an electric field, the energies of the surfaces will shift depending on orientation. The Hush[82] and PKS[83] treatments for intervalence charge transfer bands make an explicit connection between the driving force and the band position, intensity, and line width of the intervalence charge transfer transition. Since these conditions are different for each orientational subpopulation in the electric field for an isotropic sample, the Stark spectrum should not be analyzed by the classical Stark model, since the line shape depends explicitly on the driving force. In limiting cases (fully localized or fully delocalized), the classical model is a good starting point, and the value of $|\Delta\vec{\mu}|$ derived from the full nonclassical model is not too different from that obtained from the classical model; however, in many cases, the full treatment is required. The nonclassical model has been applied to the special pair cation radical, P^+, the primary product of light-induced electron transfer in the reaction center that has an intervalence charge transfer transition in the mid-IR,[94,95] and a number of inorganic mixed-valence complexes.[96] We note in passing that Stark spectra of metal-to-ligand charge transfer transitions in several high symmetry coordination complexes help to provide quantitative information on the degree of localization of these transitions.[97−102]

5. Future Directions

These Centennial Feature Articles are meant to provide a personal view and a perspective on the future, and I have emphasized work from our laboratory and how it is interconnected through the Stark effect. Many other groups have reported electronic Stark effects, for example, Stanley's work on flavins[103−106] and Peteanu's work on polyenes and electronic materials.[107−112] Electric field effects on the absorption and emission of semiconductor particles (quantum dots) and fabricated quantum wells is a huge field in science and technology that has not been mentioned at all and would include hundreds of citations. Similarly, nearly all aspects of molecular electronics are intimately connected with electric field effects, and this has recently been reviewed in this Journal.[123] I have also not described dynamic Stark experiments based on the electric field

of high intensity lasers. Like the measurements described here using conventional electric fields generated by electrodes, these novel experiments involve both spectroscopy and dynamic control of chemical reactions by the high intensity field,[113] and this promises to be an exciting area for future development.

With advances in stability and control of lasers operating in the mid-infrared, vibrational dynamics have emerged as a rich area for investigation.[114,115] The coupling between the electric field fluctuations in the environment and the oscillator is through the charge displacement (the Stark tuning rate) associated with transitions in the oscillator, making a direct connection with the work described in section 3. For example, Fayer's group used simulations of vibrational dynamics for carbon monoxide bound to the heme iron in myoglobin to extract the Stark tuning rate,[116] giving a value that is comparable to what is measured directly by vibrational Stark spectroscopy.[49] Many of the probes introduced for measurements of Stark shifts will now be studied by 2D IR methods.

The application of vibrational probes for electric fields (time-averaged or dynamic) in biological systems and comparisons with simulations is quite different from traditional areas of quantum chemistry, where a direct comparison between theory and experiment immediately benefits both (e.g., the calculation of ionization energies, gas phase spectra, structures of complexes, etc.). It is hard to overstate the impact of electrostatics calculations and simulations on our physical view of biological function and assembly, yet relatively few direct comparisons between the time-averaged electric field or the effects of fluctuations on dynamics have been made. Stark shifts are a natural bridge between these simulations and experiment and have the advantage that the information obtained is directly comparable, in contrast to other observables such as pK_a or redox potential shifts, binding constants, NMR chemical shifts, or reaction rates. Although the perfect probe remains to be developed, both static and dynamic aspects of vibrational Stark effects are likely to be an active area, especially in biological assemblies, in the coming years.

Acknowledgment. This summary of work from our laboratory is the result of contributions from many co-workers and collaborators who have used and developed Stark spectroscopy; their names can be found in the original references. I am indebted to Professor Richard Mathies, UC Berkeley, who provided advice and expertise at the start of this work and to Professor Noel Hush, University of Sydney, who has been a source of suggestions on many occasions. The work on photosynthetic systems has received sustained support from the NSF Biophysics Program; applications to nonbiological problems including the original work on vibrational Stark effects were supported by the NSF Chemistry Division; and the NIH (GM27738) supports the continuing work on the use of vibrational Stark shifts to probe protein electrostatics.

References and Notes

(1) Stark, J. *Nature* **1913**, *92*, 401. Stark, J. *Ann. Phys.* **1914**, *43*, 965.

(2) Lo Surdo, A. *Phys. Z.* **1914**, *15*, 122.

(3) The interested reader might enjoy a discussion of the parallel work and lives of Stark and Lo Surdo: Leone, M.; Paoletti, A.; Robotti, N. *Phys. Perspect.* **2004**, *6*, 271.

(4) DeLeeuv, D.; Malley, M.; Butterman, G.; Okamura, M. Y.; Feher, G. *Biophys. Soc. Abstr.* **1982**, *37*, 111a.

(5) MathiesR. A. Ph.D. Thesis, Cornell University, Ithaca, NY, 1974. Mathies, R.; Albrecht, A. C. *J. Chem. Phys.* **1974**, *60*, 2500.

(6) Mathies, R.; Stryer, L. *Proc. Natl. Acad. Sci. U.S.A.* **1976**, *73*, 2169.

(7) Liptay, W. *Angew. Chem., Int. Ed.* **1969**, *8*, 177. Liptay, W. In *Advances in Electronic Excitation and Relaxation*; Lim, E. C., Ed.; Academic Press: New York, 1974; p 129.

(8) Labhart, H. *Adv. Chem. Phys* **1967**, *13*, 179. Labhart, H. *Ber. Bunsen-Ges. Phys. Chem.* **1976**, *80*, 240.

(9) Czekalla, V. J. *Chimia* **1961**, *15*, 26.

(10) Lockhart, D. J.; Boxer, S. G. *Biochemistry* **1987**, *26*, 664.

(11) Hochstrasser, R. M. *Acc. Chem. Res.* **1973**, *6*, 263.

(12) Bublitz, G. U.; Boxer, S. G. *Annu. Rev. Phys. Chem.* **1997**, *48*, 213.

(13) Andrews, S. S. *J. Chem. Educ.* **2004**, *81*, 877.

(14) Lao, K.; Moore, L. J.; Zhou, H.; Boxer, S. G. *J. Phys. Chem.* **1995**, *99*, 496.

(15) Chattoraj, M.; King, B. A.; Bublitz, G. U.; Boxer, S. G. *Proc. Natl. Acad. Sci.* **1996**, *93*, 8362.

(16) Bublitz, G. U.; King, B. A.; Boxer, S. G. *J. Am. Chem. Soc.* **1998**, *120*, 9370.

(17) Böttcher C. J. F. *Theory of Electric Polarization*, 2nd ed.; Elsevier: Amsterdam, The Netherlands, 1973; Vol. 1.

(18) Andrews, S. S.; Boxer, S. G. *Rev. Sci. Instrum.* **2000**, *71*, 3567.

(19) Deisenhofer, J.; Epp, O.; Miki, K.; Huber, R.; Michel, H. *Nature* **1985**, *318*, 618.

(20) Ermler, U.; Fritzsch, G.; Buchanan, S. K.; Michel, H. *Structure* **1994**, *2*, 925.

(21) Chuang, J.; Boxer, S. G.; Holten, D.; Kirmaier, C. *Biochemistry* **2006**, *45*, 3845, and references therein.

(22) Lockhart, D. J.; Boxer, S. G. *Proc. Natl. Acad. Sci.* **1988**, *85*, 107.

(23) Middendorf, T. R.; Mazzola, L. T.; Lao, K.; Steffen, M. A.; Boxer, S. G. *Biochim. Biophys. Acta* **1993**, *1144*, 223.

(24) Boxer, S. G.; Goldstein, R. A.; Lockhart, D. J.; Middendorf, T. R.; Takiff, L. *J. Phys. Chem.* **1989**, *93*, 8280.

(25) McDermott, G.; Prince, S. M.; Freer, A. A.; Hawthornthwaite-Lawless, A. M.; Papiz, M. Z.; Cogdell, R. J.; Isaacs, N. W. *Nature* **1995**, *374*, 517. Green, B. R.; Parson, W. W. *Light-harvesting Antennas in Photosynthesis*; Kluwer Academic: 2003.

(26) Gottfried, D. S.; Stocker, J.; Boxer, S. G. *Biochim. Biophys. Acta* **1991**, *1059*, 6375.

(27) Beekman, L. M. P.; Steffen, M.; van Stokkum, I. H. M.; Olsen, J. D.; Hunter, C. N.; Boxer, S. G.; van Grondelle, R. *J. Phys. Chem. B* **1997**, *101*, 7284.

(28) Palacios, M. A.; Frese, R. N.; Gradinaru, C. C.; van Stokkum, I. H.; Premvardhan, L. L.; Horton, P.; Ruban, A. V.; van Grondelle, R.; van Amerongen, H. *Biochim. Biophys. Acta* **2003**, *1605*, 83.

(29) Gottfried, D. S.; Steffen, M. A.; Boxer, S. G. *Science* **1991**, *251*, 662.

(30) Gottfried, D. S.; Steffen, M. A.; Boxer, S. G. *Biochim. Biophys. Acta* **1991**, *1059*, 76..

(31) Bublitz, G. U.; Rafael Ortizm, R.; Runser, C.; Fort, A.; Barzoukas, M.; Marder, S. R.; Boxer, S. G. *J. Am. Chem. Soc.* **1997**, *119*, 2311.

(32) Bublitz, G. U.; Ortiz, R.; Marder, S. R.; Boxer, S. G. *J. Am. Chem. Soc.* **1997**, *119*, 3365.

(33) Marder, S. R.; Torruellas, W. E.; Blanchard-Desce, M.; Ricci, V.; Stegeman, G. I.; Gilmour, S.; Brédas, J.-L.; Li, J.; Bublitz, G. U.; Boxer, S. G. *Science* **1997**, *276*, 1233.

(34) Rohlfing, F.; Bradley, D. D. C. *Chem. Phys. Lett.* **1997**, *277*, 406.

(35) Karki, L.; Vance, F. W.; Hupp, J. T.; Lecours, S. M.; Therien, M. J. *J. Am. Chem. Soc.* **1998**, *120*, 2606.

(36) See, for example: Berg, J. J.; Tymoczko, J. L.; Stryer, L. *Biochemistry*; Freeman: New York, 2007; Chapter 13.

(37) Chance, B.; Smith, L. *Nature* **1955**, *175*, 803.

(38) Steffen, M. A.; Lao, K.; Boxer, S. G. *Science* **1994**, *264*, 810.

(39) Honig, B.; Dinur, U.; Nakanishi, K.; Balogh-Nair, V.; Gawinowicz, M. A.; Arnaboldi, M; Motto, M. *J. Am. Chem. Soc.* **1979**, *101*, 7084.

(40) Kakitani, T.; Honig, B.; Crofts, A. R. *Biophys. J.* **1982**, *39*, 57.

(41) Nicholls, A.; Sharp, K.; Honig, B. *Proteins: Struct., Funct., Genet.* **1991**, *11*, 281.

(42) Warshel, A.; Papazyan, A. *Curr. Opin. Struct. Biol.* **1998**, *8*, 211.

(43) Chattapadhyay, A.; Boxer, S. G. *J. Am. Chem. Soc.* **1995**, *117*, 1449.

(44) Andrews, S. S.; Boxer, S. G. *J. Phys Chem. A* **2000**, *104*, 11853.

(45) Andrews, S. S.; Boxer, S. G. *J. Phys. Chem. A* **2002**, *106*, 469.

(46) Andrews, S. S.; Boxer, S. G. *Appl. Spectrosc.* **2001**, *55*, 1161.

(47) Webb, L. J.; Boxer, S. G. *Biochemistry* **2008**, *47*, 1588.

(48) Suydam, I. T.; Boxer, S. G. *Biochemistry* **2003**, *42*, 12050.

(49) Park, E. S.; Andrews, S. S.; Hu, R. B.; Boxer, S. G. *J. Phys. Chem. B* **1999**, *103*, 9813.

(50) Varadarajan, R.; Szabo, A.; Boxer, S. G. *Proc. Natl. Acad. Sci.* **1985**, *82*, 5681.

(51) Boxer, S. G.; Wright, K. A. *J. Am. Chem. Soc.* **1979**, *101*, 6791.

(52) Varadarajan, R.; Zewart, T. E.; Gray, H. B.; Boxer, S. G. *Science* **1989**, *243*, 69.

(53) Varadarajan, R.; Lambright, D. G.; Boxer, S. G. *Biochemistry* **1989**, *28*, 3771.
(54) Park, E. S.; Thomas, M. R.; Boxer, S. G. *J. Am. Chem. Soc.* **2000**, *122*, 12297.
(55) Park, E. S.; Boxer, S. G. *J. Phys. Chem. B* **2002**, *106*, 5800.
(56) Phillips, G. N.; Teodoro, M. L.; Li, T. S.; Smith, B.; Olson, J. S. *J. Phys. Chem. B* **1999**, *103*, 8817.
(57) Suydam, I. T.; Snow, C. D.; Pande, V. S.; Boxer, S. B. *Science* **2006**, *313*, 200.
(58) Fafarman, A. T.; Webb, L. J.; Chuang, J. I.; Boxer, S. G. *J. Am. Chem. Soc.* **2006**, *128*, 13356.
(59) Sigala, P.; Fafarman, A. T.; Bogard, P. E.; Boxer, S. G.; Herschlag, D *J. Am. Chem. Soc.* **2007**, *129*, 12104.
(60) Silverman, L. N.; Pitzer, M. E.; Ankomah, P. O.; Boxer, S. G.; Fenlon, E. E. *J. Phys. Chem. B* **2007**, *111*, 11611.
(61) Krummel, A. T.; Zanni, M. T. *J. Phys. Chem. B* **2008**, *112*, 1336.
(62) Getahun, Z.; Huang, C.-Y.; Wang, T.; León, T. D.; DeGrado, W. F.; Gai, F. *J. Am. Chem. Soc.* **2003**, *125*, 405.
(63) Tucker, M. J.; Oyola, R.; Gai, F. *Biopolymers* **2006**, *83*, 571.
(64) Schultz, K. C.; Supekova, L.; Ryu, Y.; Xie, J.; Perera, R.; Schultz, P. G. *J. Am. Chem. Soc.* **2006**, *128*, 13984.
(65) Kanchanawong, C.; Case, D. A.; Romesberg, F. E *J. Am. Chem. Soc.* **2008**, *130*, 6597.
(66) Marcus, R. A.; Sutin, N. *Biochim. Biophys. Acta* **1985**, *811*, 265.
(67) Lockhart, D. J.; Boxer, S. G. *Chem. Phys. Lett.* **1988**, *144*, 243.
(68) Franzen, S.; Goldstein, R. F.; Boxer, S. G. *J. Phys. Chem.* **1990**, *94*, 5135.
(69) Lockhart, D. J.; Hammes, S. L.; Franzen, S.; Boxer, S. G. *J. Phys. Chem.* **1991**, *95*, 2217.
(70) Lockhart, D. J.; Kirmaier, C.; Holten, D.; Boxer, S. G. *J. Phys. Chem.* **1990**, *94*, 6987.
(71) Franzen, S.; Lao, K.; Boxer, S. G. *Chem. Phys. Lett.* **1992**, *197*, 380.
(72) Franzen, S.; Boxer, S. G. *J. Phys. Chem.* **1993**, *97*, 6304.
(73) Lao, K.; Franzen, S.; Stanley, R. J.; Lambright, D. G.; Boxer, S. G. *J. Phys. Chem.* **1993**, *97*, 13165.
(74) Lao, K.; Franzen, S.; Steffen, M.; Lambright, D. G.; Stanley, R. J.; Boxer, S. G. *Chem. Phys.* **1995**, *197*, 259.
(75) Lockhart, D. J.; Goldstein, R. F.; Boxer, S. G. *J. Chem. Phys.* **1988**, *89*, 1408.
(76) Franzen, S.; Stanley, R. J. *Chem. Phys.* **2002**, *276*, 115.
(77) Treynor, T. Ph.D. Thesis, Stanford University, 2003.
(78) Zhou, H.; Boxer, S. G. *J. Phys. Chem. B* **1998**, *102*, 9139.
(79) Zhou, H.; Boxer, S. G. *J. Phys. Chem. B* **1998**, *102*, 9148.
(80) Treynor, T. P.; Boxer, S. G. *J. Phys. Chem. B* **2004**, *108*, 13513.
(81) Treynor, T. P.; Boxer, S. G. *J. Phys. Chem. B* **2004**, *108*, 13523.
(82) Hush, N. S. *Prog. Inorg. Chem.* **1967**, *8*, 391.
(83) Piepho, S. B.; Krausz, E. R.; Schatz, P. N. *J. Am. Chem. Soc.* **1978**, *100*, 2996.
(84) Oh, D. H.; Boxer, S. G. *J. Am. Chem. Soc.* **1990**, *112*, 8161.
(85) Oh, D. H.; Boxer, S. G. *J. Am. Chem. Soc.* **1989**, *111*, 1130.
(86) Bublitz, G. U.; Laidlaw, W. M.; Denning, R. G.; Boxer, S. G. *J. Am. Chem. Soc.* **1998**, *120*, 6068.
(87) Karki, L.; Lu, H. P.; Hupp, J. T. *J. Phys. Chem.* **1996**, *100*, 15637–15639.
(88) Karki, L; Hupp, J. T. *J. Am. Chem. Soc.* **1997**, *110*, 4070.
(89) Vance, F. W.; Karki, L.; Reigle, J. K.; Hupp, J. T.; Ratner, M. A. *J. Phys. Chem.* **1998**, *102*, 8320.
(90) Vance, F. W.; Williams, R. D.; Hupp, J. T. *Int. Rev. Phys. Chem.* **1998**, *17*, 307.
(91) Karki, L.; Williams, R. D.; Hupp, J. T.; Allan, C. B.; Spreer, L. O. *Inorg. Chem.* **1998**, *37*, 2837.
(92) Vance, F. W.; Slone, R. V.; Stern, C. L.; Hupp, J. T. *Chem. Phys.* **2000**, *253*, 313.
(93) Treynor, T. P.; Boxer, S. G. *J. Phys. Chem. A* **2004**, *108*, 1764.
(94) Treynor, T. P.; Andrews, S. G.; Boxer, S. G. *J. Phys. Chem. B* **2003**, *107*, 11230.
(95) Kanchanawong, P.; Dahlbom, M. G.; Treynor, T. P.; Reimers, J. R.; Hush, N. S.; Boxer, S. G. *J. Phys. Chem. B* **2006**, *110*, 18688.
(96) Silverman, L. N.; Kanchanawong, P.; Treynor, T. P.; Boxer, S. G. *Philos. Trans. R. Soc. London, Ser. A* **2008**, *366*, 33.
(97) Oh, D. H.; Sano, M.; Boxer, S. G. *J. Am. Chem. Soc.* **1991**, *113*, 6880.
(98) Karki, L.; Hupp, J. T. *Inorg. Chem.* **1997**, *36*, 3318.
(99) Shin, Y. G. K.; Brunschwig, B. S.; Creutz, C.; Sutin, N. *J. Am. Chem. Soc.* **1995**, *117*, 8668.
(100) Shin, Y. G. K.; Brunschwig, B. S.; Creutz, C.; Sutin, N. *J. Phys. Chem.* **1996**, *100*, 8157.
(101) Brunschwig, B. S.; Creutz, C.; Sutin, N. *Coord. Chem. Rev.* **1998**, *177*, 61.
(102) Coe, B. J.; Harris, J. A.; Clays, K.; Persoons, A.; Wostyn, K.; Brunschwig, B. S. *Chem Commun.* **2001**, 1548.
(103) Stanley, R. J.; Jang, H. *J. Phys. Chem. A* **1999**, *103*, 8976.
(104) Stanley, R. J.; Siddiqui, M. S. *J. Phys. Chem. A* **2001**, *105*, 1100.
(105) Hopkins, N.; Stanley, R. J. *Biochemistry* **2003**, *42*, 991.
(106) Kodali, G.; Kistler, K. A.; Matsika, S.; Stanley, R. J. *J. Phys. Chem. B* **2008**, *112*, 1789.
(107) Locknar, S. A.; Peteanu, L. A. *J. Phys. Chem. B* **1998**, *102*, 4240.
(108) Premvardhan, L. L.; Peteanu, L. A. *J. Phys. Chem. A* **1999**, *103*, 7506.
(109) Locknar, S. A.; Chowdhury, A.; Peteanu, L. A. *J. Phys. Chem. B* **2000**, *104*, 5816.
(110) Premvardhan, L. L.; Wachsmann-Hogiu, S.; Peteanu, L. A.; Yaron, D. J.; Wang, P. C.; Wang, W.; MacDiarmid, A. G. *J. Chem. Phys.* **2001**, *115*, 4359.
(111) Chowdhury, A.; Locknar, S. A.; Premvardhan, L. L.; Peteanu, L. A. *J. Phys. Chem. A* **1999**, *103*, 9614.
(112) Walters, K. A.; Premvardhan, L. L.; Liu, Y.; Peteanu, L. A.; Schanze, K. S. *Chem. Phys. Lett.* **2001**, *339*, 255.
(113) Sussman, B. J.; Townsend, D.; Ivanov, M. Y.; Stolow, A. *Science* **2006**, *314*, 278.
(114) Junrong Zheng, J.; Kwak, K.; Fayer, M. D. *Acc. Chem. Res.* **2006**, *40*, 75.
(115) Zanni, M. T.; Hochstrasser, R. M. *Curr. Opin. Struct. Biol.* **2001**, *11*, 516.
(116) Finkelstein, I. J.; Goj, A.; McClain, B. L.; Massari, A. M.; Merchant, K.; Loring, R. F.; Fayer, M. D. *J. Phys. Chem. B* **2005**, *109*, 16959.
(117) Ormö, M.; Cubitt, A. B.; Kallio, K.; Gross, L. A.; Tsien, R. Y.; Remington, S. J. *Science* **1996**, *273*, 1392.
(118) Koepke, J.; Hu, X.; Muenke, C.; Schulten, K.; Michel, H. *Structure* **1996**, *4*, 581.
(119) Wild, U. P.; Bucher, S. E.; Burkhalter, F. A. *Appl. Opt.* **1985**, *24*, 1526.
(120) See, for example: Zochowski, M.; Wachowiak, M.; Falk, C. X.; Cohen, L. B.; Lam, Y-W.; Antic, S.; Zecevic, D. *Biol. Bull.* **2000**, *198*, 1.
(121) Ohta, N.; Koizumi, M.; Umeuchi, S.; Nishimura, Y.; Yamazaki, I. *J. Phys. Chem.* **1996**, *100*, 16466.
(122) Wahadoszamen, Md.; Nakabayashi, T.; Kang, S.; Imahori, H.; Ohta, N. *J. Phys. Chem. B* **2006**, *110*, 20354, and references therein.
(123) Lakshmi, S.; Dutta, S.; Pati, S. K. *J. Phys. Chem. C* **2008**, *112*, 14718.

JP8067393